Published in "Physical Review B - Condensed Matter and Materials Physics
83(17): 174407 , 2011"
which should be cited to refer to this work.

Adjusted oscillator strength matching for hybrid magnetic and electric excitations in $Dy_3Fe_5O_{12}$ garnet

P. D. Rogers,[1,*] Y. J. Choi,[2] E. C. Standard,[1] T. D. Kang,[1] K. H. Ahn,[1] A. Dubroka,[3] P. Marsik,[3] Ch. Wang,[3] C. Bernhard,[3] S. Park,[2,4] S.-W. Cheong,[2] M. Kotelyanskii,[1,5] and A. A. Sirenko[1]

[1]*Department of Physics, New Jersey Institute of Technology, Newark, New Jersey 07102, USA*
[2]*Rutgers Center for Emergent Materials and Department of Physics and Astronomy, Rutgers University, Piscataway, New Jersey 08854, USA*
[3]*Department of Physics, University of Fribourg, CH-1700 Fribourg, Switzerland*
[4]*Department of Physics, Chung-Ang University, Seoul 156-756, South Korea*
[5]*Rudolph Technologies Inc., Flanders, New Jersey 07836, USA*

Far-infrared spectra of magnetodielectric $Dy_3Fe_5O_{12}$ garnet were studied using a combination of transmittance, reflectivity, and rotating analyzer ellipsometry. In addition to purely dielectric and magnetic modes, we observed several hybrid modes with a mixed magnetic and electric dipole activity. Using 4×4 matrix formalism for materials with $\mu(\omega) \neq 1$, we modeled the experimental optical spectra and determined the far-infrared dielectric and magnetic permeability functions. The matching condition $\mu(\omega_h)S_e = \varepsilon(\omega_h)S_m$ for the oscillator strengths $S_{e(m)}$ explains the observed vanishing of certain hybrid modes at ω_h in reflectivity.

I. INTRODUCTION

Far-infrared (IR) spectra of the optical modes in magnetic materials have recently attracted a lot of attention, especially with respect to the multiferroic effect and electromagnons.[1–3] However, no universal mechanisms have been proposed to explain the occurrence of electromagnons and the accompanying magnetodielectric effect.[4,5] One challenge to theoretical modeling is its dependence on empirical data obtained with a single optical technique, such as transmittance, which, as we will see in this paper, cannot always unambiguously distinguish between electric and magnetic excitations. As we show in this paper, a combination of several complementary techniques, such as transmittance and reflectivity, for the measurements of both the complex dielectric function $\varepsilon(\omega)$ and the magnetic permeability $\mu(\omega)$ spectra can improve understanding of the coupling between magnetic and electric excitations.[6] The quantitative interpretation of the optical spectra requires an adequate modeling approach for light propagation in magnetodielectric crystals with $\mu(\omega) \neq 1$. We applied Berreman's 4×4 matrix formalism[7] for the numerical and analytic analysis of experimental data for transmittance, reflectivity, and rotating analyzer ellipsometry (RAE) in $Dy_3Fe_5O_{12}$ garnet (Dy-IG). Through the combination of these optical techniques, we determined whether an IR-active mode was (i) entirely of dielectric origin, (ii) entirely of magnetic origin, or (iii) a hybrid with a mixed electric-dipole and magnetic-dipole activity. In this paper, we show that the magnetic components of the hybrid modes are not negligibly weak and can result in a complete cancellation of the mode in reflectivity. The observed vanishing of certain hybrid modes is explained in terms of the adjusted oscillator strength matching (AOSM) condition, which has some similarities to the impedance matching phenomenon in metamaterials.[8] We also show that the RAE data, in addition to being consistent with the results of normal incidence reflectivity, illustrate that the AOSM condition is applicable for varying angles of incidence.

II. MATERIALS AND EXPERIMENTAL TECHNIQUES

The high-temperature flux growth technique was utilized to produce bulk crystals of Dy-IG ($Dy_3Fe_5O_{12}$). A sample with a (0 0 1) surface, a cross section area of 5×5 mm^2, thickness of 0.55 mm, and a 3° offset between opposite sides was used for the optical experiments. Transmittance spectra with resolution of 0.3 cm^{-1} were measured between 13 and 100 cm^{-1} at the National Synchrotron Light Source, Brookhaven National Laboratory, at the U4IR beamline equipped with a Bruker IR spectrometer, and a LHe-pumped bolometer. The RAE and reflectivity measurements were carried out at Fribourg University using an Hg lamp in the spectral range between 45 and 100 cm^{-1} with resolution of 0.7 cm^{-1}. The RAE experimental setup is similar to that described in Ref. 9. Temperature and magnetic field dependencies for static values of $\varepsilon(0,H,T)$ and $\chi(0,H,T)$ were measured using an LCR meter at 44 kHz and a SQUID magnetometer.

III. RESULTS AND ANALYSIS

Dy-IG, as well as other *RE*-IG (*RE* = Ho, Tb), is a ferrimagnetic material with a huge magnetostriction, which is related to the combination of a strong anisotropy of the crystal field of the RE^{3+} ions and a strong and anisotropic superexchange interaction between *RE* and iron.[10–13] Although there are no literature reports that Dy-IG is multiferroic, recently two related compounds, antiferromagnetic orthoferrite $DyFeO_3$ and Tb-IG, were shown to be multiferroic and magnetodielectric.[14,15] We found a magnetodielectric effect in a weak external magnetic field H of about 2 kOe. We also observed two indications of the ferromagnetic ordering of Dy spins at $T_C = 16K$: (i) the sharp minimum in the temperature derivative of magnetic susceptibility $\partial\chi/\partial T$ at T_C [Fig. 1(a)] and (ii) the temperature dependence of the exchange resonance IR mode frequencies, which will be discussed below. The quasistatic value of the dielectric constant $\varepsilon(0)$ of Dy-IG

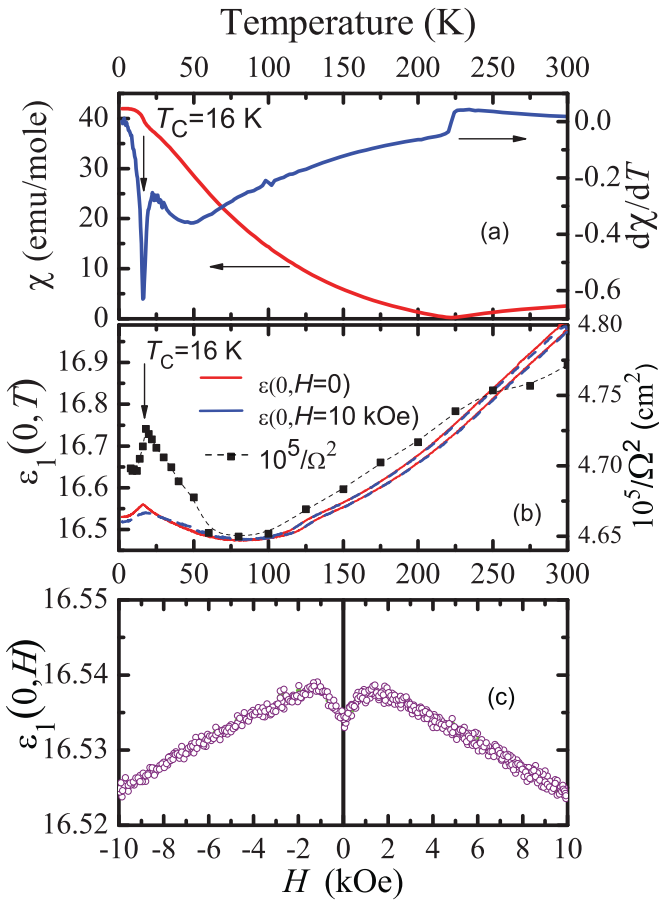

FIG. 1. (Color online) (a) Temperature dependence of the static magnetic susceptibility (red curve, left scale) and its derivative (blue curve, right scale) for a $Dy_3Fe_5O_{12}$ single crystal. Ferromagnetic ordering of Dy^{3+} occurs at $T_C = 16K$. (b) Temperature dependence of the static dielectric constant at $H = 0$ (solid red line) and $H = 10$ kOe (blue dashed line). Black squares represent the temperature dependence of the soft optical phonon frequency at 146 cm^{-1}measured with RAE. (c) Magnetic field dependence of the static dielectric constant at $T = 5$ K. In all graphs $E \parallel [1\ 0\ 0]$ and $H \parallel [0\ 1\ 1]$.

has anomalies in the temperature and external magnetic field dependencies [Figs. 1(b) and 1(c)]. $\varepsilon(0,T)$ has a peak at $T_C = 16K$ that can be explained by the local electric polarization due to antiferroelectric lattice ordering. The latter occurs in the same temperature range as the ferromagnetic ordering of the Dy spins below 16 K. The antiferroelectric lattice ordering does not create a global electric polarization, but affects the spin and lattice dynamics at the microscopic scale. Using RAE we found that the soft optical modes at $\Omega \approx 146$ and 595 cm^{-1}, which are associated primarily with Dy and oxygen displacements, contribute to the changes in $\varepsilon(0,T)$ through the Lyddane-Sachs-Teller relationship: $\varepsilon(0,T) \sim \Omega^{-2}(T)$ [see Fig. 1(b)]. The magnetodielectric effect in Dy-IG reveals itself in the variation of $\varepsilon(0,H)$ for $H < 10$ kOe [Fig. 1(c)].

The appearance of antiferroelectric ordering and a Dy−Dy ferromagnetic interaction motivates us to revisit the far-IR optical spectra of Dy-IG. *RE*-IGs have been studied in Refs. 16–19. It was shown that below 80 cm^{-1} transmission spectra in polycrystalline *RE*-IGs are dominated by both

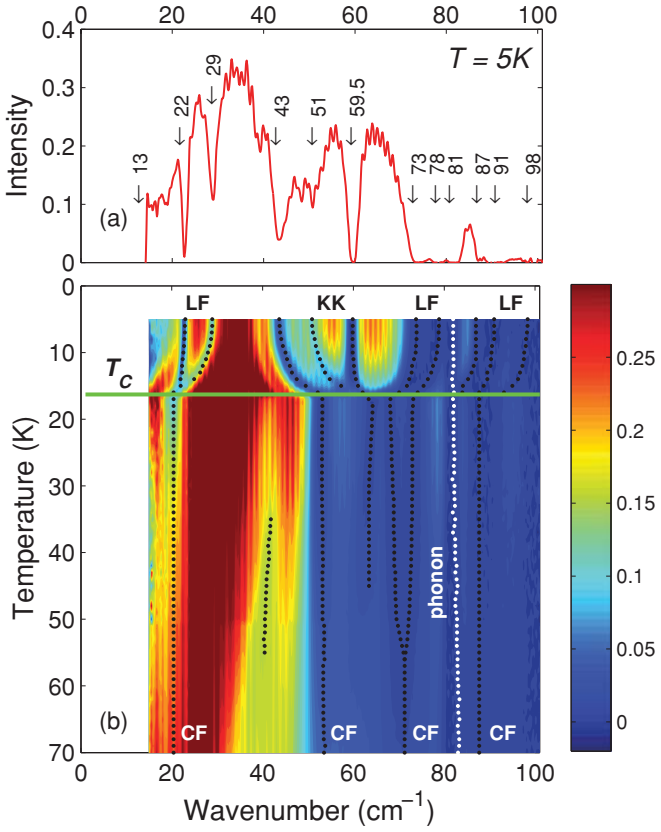

FIG. 2. (Color online) (a) Far-IR transmission spectrum for a $Dy_3Fe_5O_{12}$ single crystal measured at $T = 5$ K. The light propagation is along the [0 0 1] direction. Arrows indicate the frequencies of the IR modes. (b) Transmission map vs temperature and light frequency. The blue (dark) color corresponds to stronger absorption and red (light) color indicates high transmission. The horizontal green line represents the ferromagnetic transition temperature $T_C = 16K$. The white dots represent the phonon at 81 cm^{-1}. The black dots show the KK and LF excitations.

RE^{3+} single-ion electronic transitions and Kaplan-Kittel (KK) modes, which were attributed to magnetic dipoles.[19,20] Figures 2(a) and 2(b) show a transmittance spectrum of $Dy_3Fe_5O_{12}$ at $T = 5$ K, and the transmittance intensity map. In addition to the optical phonon at 81 cm^{-1} (see Ref. 21), a number of crystal field (CF) lines of Dy^{3+} at 20, 52, 72, and 87 cm^{-1} are observed for $T > 16$ K. At low temperatures $T < 16$ K, however, the number of absorption lines increases. The ligand field (LF) and KK modes appear at 13, 22, 29, 43, 51, 59.5, 73, 78, 87, 91, and 98 cm^{-1} for $T = 5$ K. In a simplified model for two-spin ferrimagnetic systems, like *RE*-Fe, a single exchange-type KK mode is expected with the frequency of ω_M. The LF mode ω_{LF} corresponds to precession of the Dy^{3+} moments in the effective field imposed by the iron magnetization due to the superexchange interaction between Fe and *RE*. The latter is modified by the ferromagnetic interaction between Dy^{3+} spins at low temperature. The zone-center frequencies of these collective excitations of Dy^{3+} and Fe^{3+} spins are[16,17,20]

$$\omega_M(T) = \lambda_{\text{Fe-Dy}}\mu_B[g_{\text{Dy}}M_{\text{Fe}} - g_{\text{Fe}}M_{\text{Dy}}(T)],$$
$$\omega_{\text{LF}}(T) = g_{\text{Dy}}\mu_B[\lambda_{\text{Fe-Dy}}M_{\text{Fe}} + \lambda_{\text{Dy-Dy}}M_{\text{Dy}}(T)], \quad (1)$$

where μ_B is the Bohr magneton, $\lambda_{\text{Fe-Dy}}$ is the exchange constant between Fe and Dy ions, $\lambda_{\text{Dy-Dy}}$ is the ferromagnetic exchange constant, $g_{\text{Fe}} = 2$ and g_{Dy} are the corresponding g factors, $M_{\text{Dy}}(T)$ is the Dy-sublattice magnetization, and M_{Fe} is the combined Fe magnetization. The LF and KK modes can be distinguished based on the temperature dependence of their frequencies [see Eq. (1)]. For $T < 16$ K, the KK modes $\omega_M(T)$ exhibit softening due to increase of $M_{\text{Dy}}(T)$. Figures 2(a) and 2(b) show three KK modes at 43, 51, and 59.5 cm^{-1}, that can be explained by the double umbrella structure for Dy^{3+} spins and by the strongly anisotropic and temperature-dependent superexchange interaction between Dy^{3+} and Fe^{3+} ions. The temperature-induced variation of the LF mode frequencies below 16 K is also proportional to $M_{\text{Dy}}(T)$ [see Eq. (1)], but it has an opposite sign compared to that for KK modes. Figure 2(b) indicates a phase transition at $T_C = 16K$ with appearance of the long-range ordering of Dy spins.

According to the simplified model for collinear Dy^{3+} and Fe^{3+} spins, the KK and LF modes were viewed as pure magnons.[16,17] However, their spectral proximity to the phonon at 81 cm^{-1} and modification of the LF due to local electric polarization should result in a hybrid electric-dipole and magnetic-dipole activity. In the following, we will prove this suggestion using a combination of several optical techniques: transmittance and reflectivity at normal incidence and RAE. The terms "LF" and "hybrid" will be applied interchangeably to the same modes. The first term refers to the origin of the IR-active excitation as described above, while the latter corresponds to the mixed dipole activity of the mode in the optical spectra.

Figures 3(a) and 3(b) compare the transmittance $T_s(\omega)$ and reflectivity $R_s(\omega)$ spectra of the same Dy-IG sample as in Fig. 2. $T_s(\omega)$ and $R_s(\omega)$ have been measured at $T = 8$ and 9 K, respectively, at near-normal incidence, that is, the angle of incidence (AOI) is close to zero. RAE measurements were taken for the same sample at $T = 8$ K and AOI = 75 deg. The results of the RAE measurements are shown in terms of the real part of the pseudodielectric function $\langle\varepsilon_1(\omega)\rangle$ [Fig. 3(c)]. Modes of three kinds can be identified in Figs. 3(a)–3(c). (i) The phonon at 81 cm^{-1}, which is obviously an electric dipole, has a conventional Lorentz shape in the $R_s(\omega)$ and RAE spectra. The phonon is also strong in $T_s(\omega)$. (ii) The KK mode at 59.5 cm^{-1} has an inverted Lorentz shape in both the $R_s(\omega)$ and RAE spectra. As shown below, this shape is typical for magnetic dipoles. (iii) The LF modes at 73, 78, and 91 cm^{-1} are as strong as the phonon in $T_s(\omega)$, but practically invisible in both the $R_s(\omega)$ and RAE spectra. The $T_s(\omega)$ and $R_s(\omega)$ spectra, both measured for the same sample and at the same AOI, can be reconciled by suggesting that the LF modes in Dy-IG possess a hybrid, that is, magnetic-dipole and electric-dipole activity. This suggestion can be qualitatively understood based on Veselago's approach for light propagation in an isotropic, semi-infinite medium with $\mu(\omega) \neq 1$. Here a simple replacement of the refractive index is used: for Fresnel's reflection coefficient $n(\omega) \to \sqrt{\varepsilon(\omega)/\mu(\omega)}$; while in transmittance $n(\omega) \to \sqrt{\varepsilon(\omega)\cdot\mu(\omega)}$.[22] These formulas explain that a magnetic mode has an inverted shape in the reflectivity spectrum since $n(\omega) \sim \sqrt{1/\mu(\omega)}$ in the vicinity of the mode where $\varepsilon(\omega) \approx$ const. They also naturally account for the suppression of the mode feature in the reflectivity

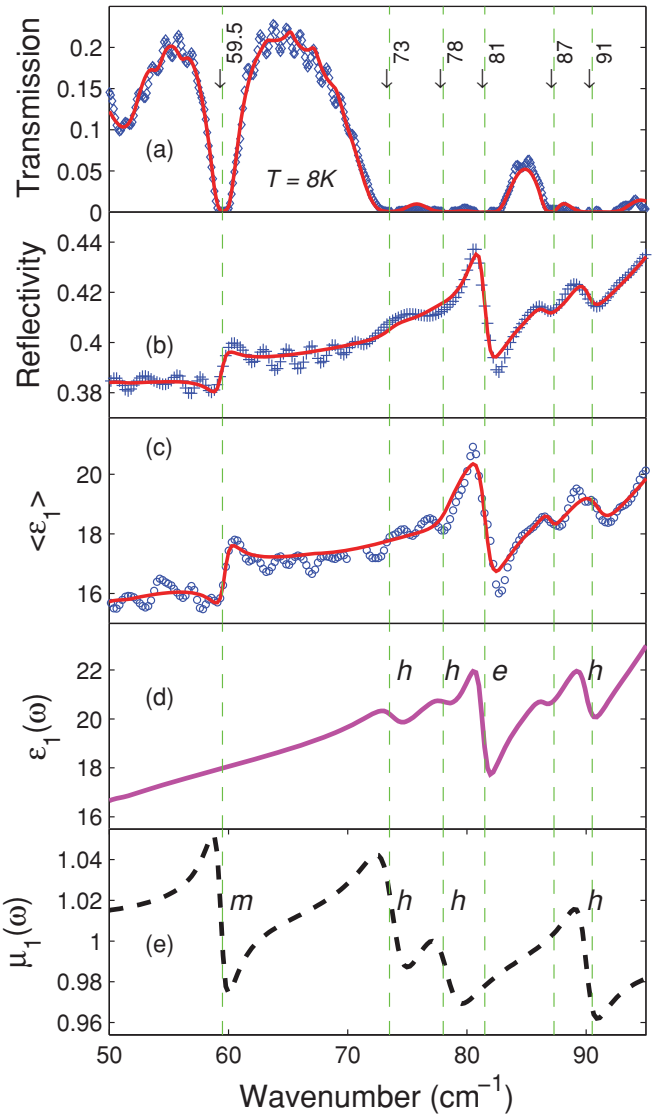

FIG. 3. (Color online) Optical spectra of a $Dy_3Fe_5O_{12}$ single crystal. (a) Transmission spectrum at AOI = 0, $T = 8$ K. (b) Absolute far-IR reflectivity at AOI = 0, $T = 9$ K. (c) Rotating analyzer ellipsometry (RAE) data for pseudodielectric function $\langle\varepsilon_1(\omega)\rangle$ at AOI = 75 deg, $T = 8$ K. In (a), (b), and (c) the blue diamonds are experimental data and the red solid curves represent results of the fit. Electric (d) and magnetic (e) susceptibilities as determined from the fit results. Magnetic, electric, and hybrid modes are marked with *m*, *e*, and *h*, respectively.

spectrum for a hybrid, that is, magnetic-dielectric mode, where the magnetic and dielectric components tend to cancel each other (see the Appendix for further details).

In order to properly analyze the experimental data in Figs. 3(a)–3(c), we developed an exact numeric method (see Ref. 23 for details), which is based on Berreman's 4×4 matrix formalism.[7,23] Our method incorporates the exact geometry of the measured Dy-IG sample with average thickness $d =$ 0.55 mm, multiple reflections, variable AOI's, and possible magnetic and electric anisotropies. The response functions of

TABLE I. The values of parameters of optical phonon at 81 cm^{-1} (e), magnetic KK mode at 59.5 cm^{-1} (m), and three hybrid modes (h) at 73, 78 and 91 cm^{-1} obtained from the analysis of the combination of the transmission, RAE and reflectivity measurements.

ω_0 (cm^{-1})	S_e	S_m	Type
59.5	–	0.0019	m
73	0.036	0.0021	h
78	0.035	0.0022	h
81	0.077	–	e
91	0.032	0.0010	h

Dy-IG, $\varepsilon(\omega)$ and $\mu(\omega)$, were modeled using a set of Lorentz oscillators:

$$\varepsilon(\omega) = \varepsilon_\infty + \sum_{j=1}^{N} \frac{S_{j,e}\omega_{j,e0}^2}{\omega_{j,e0}^2 - \omega^2 - i\gamma_{j,e}\omega},$$

$$\mu(\omega) = \mu_\infty + \sum_{j=1}^{M} \frac{S_{j,m}\omega_{j,m0}^2}{\omega_{j,m0}^2 - \omega^2 - i\gamma_{j,m}\omega}. \quad (2)$$

Here ε_∞ is the infinite-frequency value of the dielectric function $\mu_\infty \cong 1$, $S_{e(m)}$ is the oscillator strength, $\gamma_{e(m)}$ is the damping constant, and $\omega_{e(m)0}$ is the resonance frequency. Although the response functions of Dy-IG can be in principle anisotropic, the comparison of the reflectivity and ellipsometric data taken at different AOI do not reveal any anisotropy within the accuracy of the data. The hybrid modes in this model have nonzero electric and magnetic oscillator strengths S_e and S_m at the same resonant frequency $\omega_h = \omega_{e(m)0}$, thus creating a contribution to both $\varepsilon(\omega)$ and $\mu(\omega)$. The electric and magnetic damping constants for the hybrid modes are assumed to be the same: $\gamma_e = \gamma_m$. The results of the fit using 4×4 matrix formalism for $R_s(\omega)$, $T_s(\omega)$, and $\langle\varepsilon_1(\omega)\rangle$ are shown in Figs. 3(a)–3(c) with solid curves. The corresponding values of S_e and S_m are summarized in Table I and the real parts of the dielectric function and the magnetic permeability are shown in Figs. 3(d) and 3(e). Note that for Dy-IG, S_e and S_m are not large enough to modify significantly the background values of $\varepsilon_\infty \cong 17$ and $\mu_\infty \cong 1$. Hence, both $\varepsilon(\omega)$ and $\mu(\omega)$ are positive everywhere in the vicinity of the hybrid mode frequencies [see Figs. 3(d) and 3(e)]. Thus, the natural occurrence of a negative index of refraction does not take place at the spectral range dominated by the hybrid modes that might otherwise occur if their damping were sufficiently low.

Certain analytical formulas can be obtained which assist in describing the measured $T_s(\omega)$, $R_s(\omega)$, and RAE spectra. Consider two electric and magnetic oscillators that are separated on the energy scale and have comparable values of $\gamma_e \approx \gamma_m$. If the backside reflection is not strong, the ratio of the amplitudes of the modes in the reflectivity spectra at their respective resonances are related to $\partial R_{ss}(\omega)/\partial\omega|_{\omega e(m)0}$ as follows:

$$\frac{\partial R_{ss}/\partial\omega|_{\omega e0}}{\partial R_{ss}/\partial\omega|_{\omega m0}} \approx -\frac{\mu_\infty}{\varepsilon_\infty}\frac{S_e}{S_m}\frac{\omega_{e0}}{\omega_{m0}}, \quad (3)$$

where $S_e \ll \varepsilon_\infty$. μ_∞ and ε_∞ are determined at the frequencies shifted from $\omega_{e(m)0}$ by at least $3\gamma_{e(m)}$. Note that the negative sign corresponds to the inverted Lorentzian shape at the magnetic resonance. If the thickness of the sample d is optimized to prevent saturation of the transmitted intensity at the resonance, then the following relationship for transmission amplitudes of the magnetic and electric modes can be obtained:

$$\frac{\Delta T_e}{\Delta T_m} \approx \frac{\mu_\infty}{\varepsilon_\infty}\frac{S_e}{S_m}\frac{\omega_{e0}^2}{\omega_{m0}^2}, \quad (4)$$

where $\Delta T_{e(m)} \approx T(\omega_{e(m)0}) - T(\omega_{e(m)0} \pm 3\gamma_{e(m)})$. In the case of hybrid modes with a mixed electric-dipole and magnetic-dipole activity, Eqs. (3) and (4) indicate that the contribution of the dielectric and magnetic oscillators to the transmission spectra is additive with an adjusted oscillator strength (AOS) $S_T \approx \mu_\infty \cdot S_e + \varepsilon_\infty \cdot S_m$, while their total contribution to reflectivity is subtractive with AOS of $S_R = (\mu_\infty \cdot S_e - \varepsilon_\infty \cdot S_m)/\mu_\infty^2$. Here the relevant magnetic or dielectric oscillator strength is multiplied by its constitutive response function complement. For the general case of a spectrum with several hybrid modes, a complete cancellation in reflectivity measurements is possible for each mode if the adjusted oscillator strength matching condition (AOSM) occurs: $\mu(\omega_h) \cdot S_e = \varepsilon(\omega_h) \cdot S_m$. These results are consistent with the aforementioned Veselago approach (see the Appendix). In our experiment the AOSM condition is realized for the hybrid modes at 73 and 78 cm^{-1} that are not visible in either normal-incidence reflectivity or RAE experiments. The hybrid mode contribution to $dR_{ss}(\omega_h)/d\omega$ is negligible and the $R_s(\omega)$ spectrum looks essentially featureless around the resonance frequencies. Analysis of RAE spectra taken at AOI = 75° shows that the AOSM condition $\mu(\omega_h) \cdot S_e \approx \varepsilon(\omega_h) \cdot S_m$ is valid across a wide range of AOIs, even close to the Brewster angle (76.4° for $\varepsilon_\infty = 17$ and $\mu_\infty = 1$).

IV. CONCLUSIONS

In conclusion, the rare occurrence of the AOSM condition for hybrid modes was studied in Dy-IG. The proximity of the Dy^{3+} LF exchange resonances (73 and 78 cm^{-1}) to the frequency of the lowest optical phonon (81 cm^{-1}), local electric polarization, and the noncollinear spin structure for the Dy-Fe magnetic system are responsible for the mode hybridization. The AOSM condition is used to explain the almost complete cancellation of the hybrid modes in the reflectivity spectra while remaining strong in the transmission spectra. One of the possible applications of the AOSM condition is for the design of antireflective coatings in the far-IR spectral range using magnetic materials and metamaterials.

ACKNOWLEDGMENTS

The authors are thankful to T. Zhou, G. L. Carr, and C. Homes for discussions. The transmission experiments at NJIT and the crystal growth at Rutgers were supported by DOE DE-FG02-07ER46382. Use of the NSLS-BNL was supported by DOE DE-AC02-98CH10886. The measurements at University of Fribourg were supported by LiMAT and by SNF Grants 200020-129484 and the NCCR-MaNEP. Development of 4×4 matrix formalism was supported by NSF-DMR-0821224.

APPENDIX

Expressions for the adjusted oscillator strength (AOS) and the adjusted oscillator strength matching (AOSM) condition are developed for materials with $\mu \neq 1$. Veselago's results for semi-infinite magnetic materials[22,24] together with analytic expressions obtained by the authors in Ref. 23 are used in this treatment. A Lorentzian oscillator model is used in the formulas below for magnetic and dielectric excitations. For a single-hybrid excitation, the dielectric and magnetic contributions are given in Eq. (2), where $N = M = 1$, $\omega_{e0} = \omega_{m0} = \omega_h$, and $\gamma_e = \gamma_m = \gamma$.

The semi-infinite case for normal incident radiation (AOI = 0) is examined first. Based on Veselago's work, it is assumed that the s polarized reflection intensity $R_{ss}(\omega)$ is a function of $\sqrt{\varepsilon(\omega)/\mu(\omega)}$.[22,24] Then, in the proximity of a resonance with a single hybrid mode

$$\begin{aligned} R_{ss}(\omega) &= f\left(\sqrt{\frac{\varepsilon(\omega)}{\mu(\omega)}}\right) = f\left(\sqrt{\frac{\varepsilon_\infty + \frac{S_e\omega_h^2}{\left(\omega_h^2-\omega^2-i\gamma\omega\right)}}{\mu_\infty + \frac{S_m\omega_h^2}{\left(\omega_h^2-\omega^2-i\gamma\omega\right)}}}\right) \\ &\approx f\left(\sqrt{\frac{\varepsilon_\infty}{\mu_\infty} + \frac{\left(\mu_\infty S_e - \varepsilon_\infty S_m\right)\omega_h^2}{\mu_\infty^2\left(\omega_h^2-\omega^2-i\gamma\omega\right)}}\right) \\ &= f\left(\sqrt{\frac{\varepsilon_\infty}{\mu_\infty} + \frac{S_R\omega_h^2}{\left(\omega_h^2-\omega^2-i\gamma\omega\right)}}\right), \end{aligned} \tag{A1}$$

where $f(x) = |(1-x)/(1+x)|^2$. The expansion in Eq. (A1) is justified since $S_m \ll \mu_\infty$ for the magnetic modes (see Table I).

In general, the hybrid resonance can be described with an AOS in reflection: $S_R = (\mu_\infty S_e - \varepsilon_\infty S_m)/\mu_\infty^2$. We have also derived a similar expression for S_R by analyzing the derivative of the exact complex reflection coefficient with respect to frequency for the thin film configuration, which will be described below. The AOSM condition $S_m\varepsilon_\infty = S_e\mu_\infty$ is immediately apparent from Eq. (A1). Under this condition, the hybrid mode disappears from reflectivity and reflectivity becomes a function of ε_∞ and μ_∞ only: $R_{ss}(\omega_h) = f(\sqrt{\varepsilon_\infty/\mu_\infty})|_{S_m\varepsilon_\infty = S_e\mu_\infty}$.

For a pure magnetic dipole at $\omega_h = \omega_{m0}$, Eq. (A1) can be approximated for $S_e = 0$ and $\mu_\infty = 1$ as

$$\begin{aligned} R_{ss}(\omega) &= f\left\{\sqrt{\varepsilon_\infty - \frac{\varepsilon_\infty S_m\omega_m^2}{\left[\omega_{m0}^2(1+S_m) - \omega^2 - i\gamma\omega\right]}}\right\} \\ &\approx f\left(\sqrt{\varepsilon_\infty - \frac{\varepsilon_\infty S_m\omega_m^2}{\left(\omega_{\mathrm{LO}}^2 - \omega^2 - i\gamma\omega\right)}}\right). \end{aligned} \tag{A2}$$

The negative sign in Eq. (A2) corresponds to the inverted Lorentzian shape of a pure magnetic dipole with AOS: $S_R = S_m\varepsilon_\infty$. For hybrid modes this inverted shape provides for the partial or complete cancellation of the electric and magnetic components at resonance. As is evident from Eq. (A2), a pole in the effective dielectric function measured, for example, in RAE experiments, is shifted from ω_{m0}, appearing at the longitudinal frequency $\omega_{\mathrm{LO}} = \omega_{m0}\sqrt{1+S_m}$. Note that this frequency shift is small due to $S_m \ll \mu_\infty$ for magnetic modes.

If light propagation in transmission is mainly driven by exponential decay and the extinction coefficient, according to Veselago, $T_{ss}(\omega)$ becomes a function of the product $\varepsilon(\omega)\cdot\mu(\omega)$:

$$\begin{aligned} T_{ss}(\omega) &= F[\sqrt{\varepsilon(\omega)\cdot\mu(\omega)}] \\ &= F\left\{\sqrt{\left[\varepsilon_\infty + \frac{S_e\omega_h^2}{\left(\omega_h^2-\omega^2-i\gamma\omega\right)}\right]\cdot\left[\mu_\infty + \frac{S_m\omega_h^2}{\left(\omega_h^2-\omega^2-i\gamma\omega\right)}\right]}\right\} \\ &= F\left[\sqrt{\varepsilon_\infty\cdot\mu_\infty + \frac{\left(S_e\cdot\mu_\infty + S_m\cdot\varepsilon_\infty\right)\cdot\omega_h^2}{\left(\omega_h^2-\omega^2-i\gamma\omega\right)} + \delta}\right] \\ &\approx F\left[\sqrt{\varepsilon_\infty + \frac{S_T\cdot\omega_h^2}{\left(\omega_h^2-\omega^2-i\gamma\omega\right)}}\right]. \end{aligned} \tag{A3}$$

For strong absorption at the hybrid mode, when one can neglect multiple reflections $F(y) = |(1-r^2)t(y)|^2$, where $y = \sqrt{\varepsilon\cdot\mu}$, $t(y) = \exp(i\frac{\omega}{c}yd)$, and r is the complex reflection coefficient. We note that at ω_h, the reflection intensity $R(\omega)$ as described by Eq. (A1) does not change significantly. As one can see from Eq. (A3), the AOS in transmission is $S_T \approx S_e\cdot\mu_\infty + S_m\cdot\varepsilon_\infty$. In contrast to S_R, the magnetic and electric oscillator strengths in S_T are additive. Note that the contribution of the magnetic oscillator strength in S_T is "enhanced" by ε_∞. The expressions for S_R and S_T allow for analysis of the interesting case of hybrid modes which can cancel or disappear in reflectivity but remain strong in transmission. Note that the exact analytical expression for $F(y)$ in the general case of multiple reflections is complicated and will be discussed below.

A complete analysis of thin film reflectivity and transmission must involve the reflection from the backside of the sample, which depends on the thickness d. The opposing shapes of the Lorentzian profile of the magnetic and electric excitations motivate the calculation of $\frac{\partial R_{ss}(\omega_h)}{\partial\omega}$ and $\frac{dT_{ss}(\omega_h)}{d\omega}$. The two total derivatives require partial derivative expansion of the response functions as well as those of r_{ss} and t_{ss}, the complex

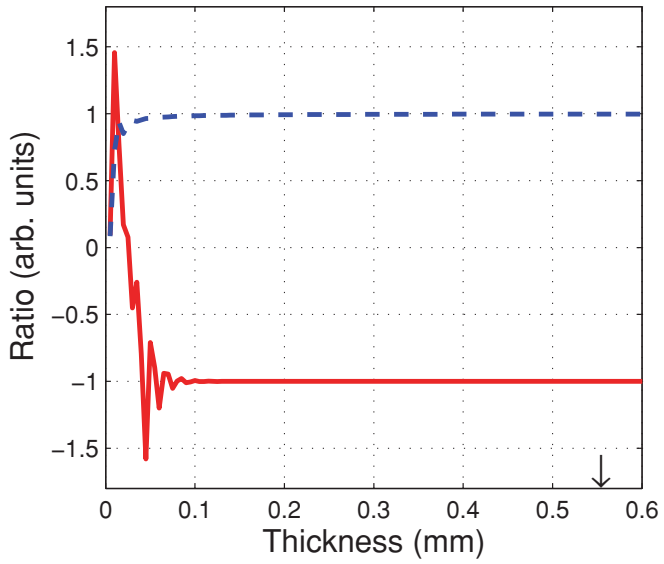

FIG. 4. (Color online) Variability of the ratio of α terms with thin film thickness d. $\varepsilon_\infty = 15.85$, $S_e = 0.100$, $S_m = 0.0063$, and $\omega_h = 78\,\mathrm{cm}^{-1}$. $\frac{\alpha_m^{R_{TF}}(\omega_h)}{\alpha_e^{R_{TF}}(\omega_h)}$ is the bottom solid red line. $\frac{\alpha_m^{T}(\omega_h)}{\alpha_e^{T}(\omega_h)}$ is the top blue dashed line. For the $Dy_3Fe_5O_{12}$ sample with thickness $d = 0.55$ mm, the opposite signs of these two ratios account for the subtraction of AOS contributions in reflectivity and the addition of the AOS contributions in transmission.

reflection and transmission coefficients. For a magnetic thin film whose principal axes are coincident with the laboratory system, r_{ss} and t_{ss} are given by[23]

$$r_{ss} = \frac{q_{zs}\cos(q_{zs}d)(k_{z0}-k_{z2}) + i\left(\frac{q_{zs}^2}{\mu_{xx}} - k_{z0}k_{z2}\mu_{xx}\right)\sin(q_{zs}d)}{q_{zs}\cos(q_{zs}d)(k_{z0}+k_{z2}) - i\left(\frac{q_{zs}^2}{\mu_{xx}} + k_{z0}k_{z2}\mu_{xx}\right)\sin(q_{zs}d)}$$
$$t_{ss} = \frac{2k_{z0}q_{zs}}{q_{zs}\cos(q_{zs}d)(k_{z0}+k_{z2}) - i\left(\frac{q_{zs}^2}{\mu_{xx}} + k_{z0}k_{z2}\mu_{xx}\right)\sin(q_{zs}d)}, \tag{A4}$$

where k_{z0}, q_{zs}, and k_{z2} are the z components of the wave vector in the incident, thin film, and substrate media, respectively. At hybrid resonance, the following expressions for the two total derivatives are obtained:

$$\frac{dR_{ss}}{d\omega} \cong r_{ss}^* \cdot S_2 + r_{ss} \cdot S_2^* \quad \text{and} \quad \frac{dT_{ss}}{d\omega} \cong t_{ss}^* \cdot S_3 + t_{ss} \cdot S_3^*. \tag{A5}$$

where S_2 and S_3 are given by

$$S_2 = -\frac{2\omega_h}{\gamma_h^2}\frac{\alpha_e^{R_{TF}}(\omega_h)}{\sqrt{\mu(\omega_h)\,\varepsilon(\omega_h)}} \times \left[\mu(\omega_h)\,S_e + \varepsilon(\omega_h)\,S_m\frac{\alpha_m^{R_{TF}}(\omega_h)}{\alpha_e^{R_{TF}}(\omega_h)}\right], \tag{A6}$$
$$S_3 = -\frac{2\omega_h}{\gamma_h^2}\frac{\alpha_e^{T}(\omega_h)}{\sqrt{\mu(\omega_h)\,\varepsilon(\omega_h)}}\left[\mu(\omega_h)\,S_e + \varepsilon(\omega_h)\,S_m\frac{\alpha_m^{T}(\omega_h)}{\alpha_e^{T}(\omega_h)}\right].$$

The four α terms are components of the partial derivatives of the complex reflection and transmission coefficients taken with respect to the two response functions. Analytic solutions for these terms can be obtained starting from r_{ss} and t_{ss}. For the material parameters of $Dy_3Fe_5O_{12}$ sample with the thickness of 0.55 mm, $\frac{\alpha_m^{R_{TF}}(\omega_h)}{\alpha_e^{R_{TF}}(\omega_h)}$ and $\frac{\alpha_m^{T}(\omega_h)}{\alpha_e^{T}(\omega_h)}$ are negative and positive, respectively, with absolute value equal to 1 (see Fig. 4). When these values are inserted into Eq. (A6), the upper and lower bracketed terms can be identified with the S_R and S_T terms discussed in the Veselago qualitative analysis above. These results are also consistent with the subtraction and addition of the AOS components in reflectivity and transmission, respectively.

The case where hybrid mode magnetic and electric dipole contributions completely cancel in reflection ($S_R = 0$) but add to S_T in transmission requires the solution of the following simultaneous equation:

$$\mu(\omega_h)\,S_e + \varepsilon(\omega_h)\,S_m\frac{\alpha_m^{R_{TF}}(\omega_h)}{\alpha_e^{R_{TF}}(\omega_h)} = 0,$$
$$\mu(\omega_h)\,S_e + \varepsilon(\omega_h)\,S_m\frac{\alpha_m^{T}(\omega_h)}{\alpha_e^{T}(\omega_h)} = S_T. \tag{A7}$$

For the case of the fitted parameters for Dy-IG, $\frac{\alpha_m^{R_{TF}}(\omega_h)}{\alpha_e^{R_{TF}}(\omega_h)} \approx -1$, $\frac{\alpha_m^{T}(\omega_h)}{\alpha_e^{T}(\omega_h)} \approx 1$, $\mu(\omega_h) \approx 1$, and $\varepsilon(\omega_h) \approx \varepsilon_\infty$, Eq. (A7) has the approximate solution: $S_e \cong \frac{S_T}{2}$ and $S_m \cong \frac{S_T}{2\varepsilon_\infty}$.

*pdr2@njit.edu

[1] A. Pimenov, A. A. Mukhin, V. Y. Ivanov, V. D. Travkin, A. M. Balbashov, and A. Loidl, Nat. Phys. **2**, 97 (2006).

[2] A. B. Sushkov, R. V. Aguilar, S. Park, S. W. Cheong, and H. D. Drew, Phys. Rev. Lett. **98**, 027202 (2007).

[3] Y. Takahashi, N. Kida, Y. Yamasaki, J. Fujioka, T. Arima, R. Shimano, S. Miyahara, M. Mochizuki, N. Furukawa, and Y. Tokura, Phys. Rev. Lett. **101**, 187201 (2008).

[4] R. Valdes Aguilar, M. Mostovoy, A. B. Sushkov, C. L. Zhang, Y. J. Choi, S. W. Cheong, and H. D. Drew, Phys. Rev. Lett. **102**, 047203 (2009).

[5] Y. Takahashi, S. Ishiwata, S. Miyahara, Y. Kaneko, N. Furukawa, Y. Taguchi, R. Shimano, and Y. Tokura, Phys. Rev. B **81**, 100413 (2010).

[6] A. M. Nicholson and G. F. Ross, IEEE Trans. Instrum. Meas. **IM-19**, 377 (1970).

[7] D. W. Berreman, J. Opt. Soc. Am. **62**, 502 (1972).

[8] A. N. Grigorenko, A. K. Geim, H. F. Gleeson, Y. Zhang, A. A. Firsov, I. Y. Khrushchev, and J. Petrovic, Nature (London) **438**, 335 (2005).

[9] C. Bernhard, J. Humlícek, and B. Keimer, Thin Solid Films **455-456**, 143 (2004).

[10]F. Sayetat, J. Magn. Magn. Mater. **58**, 334 (1986).
[11]K. P. Belov and V. I. Sokolov, Sov. Phys. Usp. **20**, 149 (1977).
[12]R. Hock, H. Fuess, T. Vogt, and M. Bonnet, J. Solid State Chem. **84**, 39 (1990).
[13]M. Lahoubi, M. Guillot, A. Marchand, F. Tcheou, and E. Roudault, IEEE Trans. Mag. **20**, 1518 (1984).
[14]Y. Tokunaga, S. Iguchi, T. Arima, and Y. Tokura, Phys. Rev. Lett. **101**, 097205 (2008).
[15]N. Hur, S. Park, S. Guha, A. Borissov, V. Kiryukhin, and S.-W. Cheong, Appl. Phys. Lett. **87** (2005).
[16]A. J. Sievers and M. Tinkham, Phys. Rev. **129**, 1995 (1963).
[17]M. Tinkham, Phys. Rev. **124**, 311 (1961).
[18]J. Yamamoto, B. T. Smith, and E. E. Bell, J. Opt. Soc. Am. **64**, 880 (1974).
[19]T. D. Kang, E. Standard, K. H. Ahn, A. A. Sirenko, G. L. Carr, S. Park, Y. J. Choi, M. Ramazanoglu, V. Kiryukhin, and S. W. Cheong, Phys. Rev. B **82**, 014414 (2010).
[20]J. Kaplan and C. Kittel, J. Chem. Phys. **21**, 760 (1953).
[21]N. T. McDevitt, J. Opt. Soc. Am. **59**, 1240 (1969).
[22]V. G. Veselago, Sov. Phys. Usp. **10**, 509 (1968).
[23]P. D. Rogers, T. D. Kang, T. Zhou, M. Kotelyanskii, and A. A. Sirenko, Thin Solid Films **519**, 2668 (2011).
[24]V. Veselago, L. Braginksy, V. Shklover, and C. Hafner, J. Comput. Theor. Nanosci. **3**, 1 (2006).